物理化学学报(Wuli Huaxue Xuebao)
第 27 卷第 12 期(2011 年 12 月)

目　　次

(下转封三)

(上接封二)

光化学和辐射化学

生物物理化学

材料物理化学

新闻与评述

ACTA PHYSICO-CHIMICA SINICA
Vol. 27 No.12 (December, 2011)

COVER

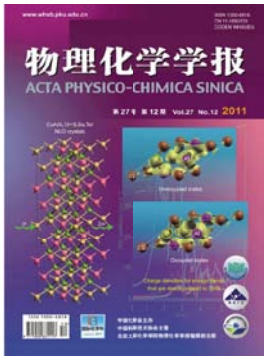

The cover image presents the structure, the charge density maps associated with the mechanism of second harmonic generation (SHG), and the frequency-dependent of SHG coefficient of the chalcopyrite-type $CuAlX_2$ (X=S, Se, Te) semiconductors. On page 2805, ZHOU *et al*. demonstrate that the SHG response of $CuAlX_2$ is mainly related to the transitions from the occupied bands near the top of the valence band to the unoccupied bands that are dominated by valence *p* states of Al and X atoms.

CONTENTS

THERMODYNAMICS, KINETICS, AND STRUCTURE CHEMISTRY

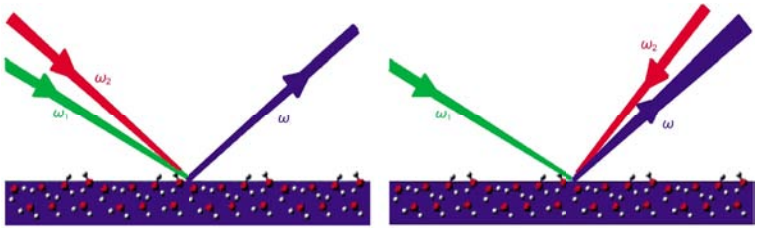

Co-propagating and counter-propagating experimental configurations for SFG-VS (DFG-VS) give different signal dispersion angles and detection efficiencies.

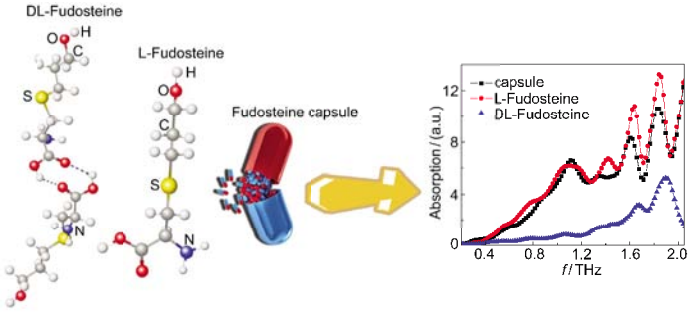

THz-TDS can be used to discriminate L- and DL-Fudosteine and to determine the main components of the Fudosteine capsule.

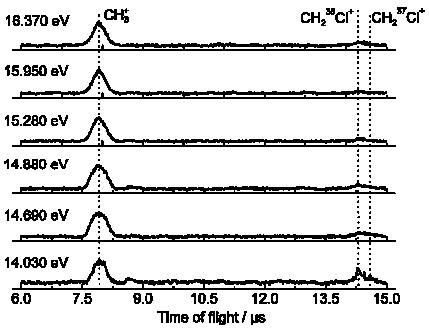

CH_3^+ formation pathways from the CH_3Cl^+ (A^2A_1 and B^2E) ions are of the rapid direct and statistical dissociation types, respectively.

Mechanism Construction and Simulation for the High-Temperature Combustion of *n*-Dodecane

HUA Xiao-Xiao WANG Jing-Bo
WANG Quan-De TAN Ning-Xin
LI Xiang-Yuan

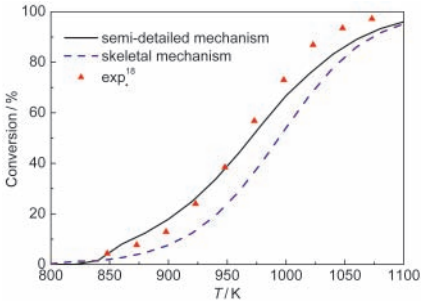

A semi-detailed mechanism and a skeletal mechanism for the high-temperature combustion of *n*-dodecane were developed and validated.

Acta Phys. -Chim. Sin. **2011,** *27* (12), 2755−2761

Dynamic Viscosity and Conductivity of Ionic Liquids [$C_n$py][NTf_2] (*n*=2, 4, 5)

LIU Qing-Shan YAN Pei-Fang
YANG Miao TAN Zhi-Cheng
LI Chang-Ping WELZ-BIERMANN Urs

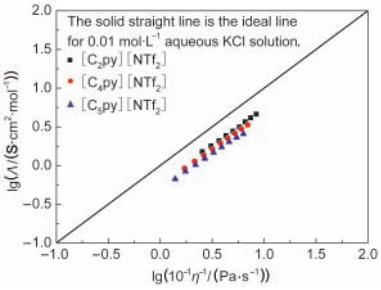

The dynamic viscosity and conductivity of the ILs [$C_n$py][NTf_2] (*n*= 2, 4, 5) were determined from 283.15 to 338.15 K; the relationship between the molar conductivity, Λ, and dynamic viscosity, η, was described in terms of Walden′s rule.

Acta Phys. -Chim. Sin. **2011,** *27* (12), 2762−2766

Adsorption Performance of Tetradecyl Aryl Sulfonates on Oil Sand from the Daqing Oilfield

DONG Zhi-Long DING Wei
LIU Kun ZHANG Zhi-Wei
QU Guang-Miao YU Tao

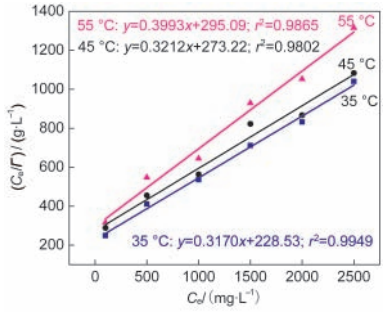

The relationship between the structural isomers of sulfonates determines their properties.

Acta Phys. -Chim. Sin. **2011,** *27* (12), 2767−2772

Dissociation Conditions and Influencing Factors of Methane Hydrate in Chloride Salt Solution under High Pressure

SUN Shi-Cai LIU Chang-Ling
YE Yu-Guang JIANG Qian

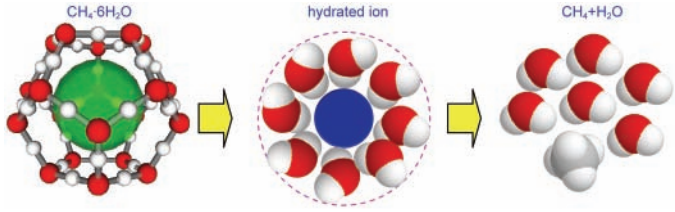

Acta Phys. -Chim. Sin. **2011,** *27* (12), 2773−2778

Methane hydrate decomposes more easily under the hydrated ion effect.

THEORETICAL AND COMPUTATIONAL CHEMISTRY

Car-Parrinello Molecular Dynamics Simulations of Microstructure Properties of Liquid Water, Methanol and Ethanol

ZENG Yong-Ping ZHU Xiao-Min
YANG Zheng-Hua

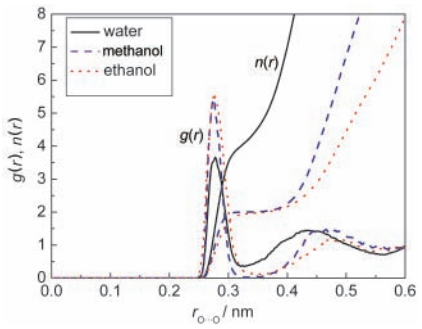

Car-Parrinello molecular dynamics was performed on the solvent structure properties of water, methanol, and ethanol. Different hydrogen-bonded network structures are formed *via* hydrogen bonds. The hydrophobic groups have an important effect on the structural properties.

Acta Phys. -Chim. Sin. **2011,** *27* (12), 2779−2785

Meaning and Functional Form of the Electron Localization Function

LU Tian CHEN Fei-Wu

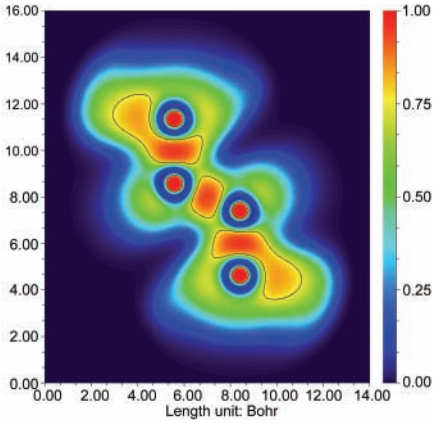

The physical background of the electron localization function is discussed in detail. Some incorrect uses of this function in the literature are pointed out.

Acta Phys. -Chim. Sin. **2011,** *27* (12), 2786−2792

First-Principles Calculation of the Crystal Structure and Stabilization of Mg-Ti-H System

DU Xiao-Ming LI Wu-Hui
HUANG Yong WU Er-Dong

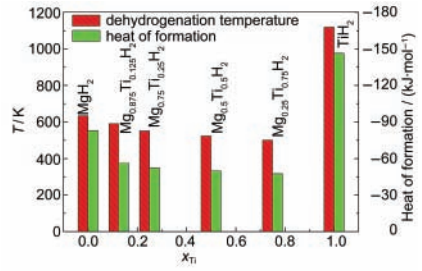

Titanium can reduce the stabilization and dehydrogenation temperatures of $Mg_xTi_{(1-x)}H_2$ hydrides and play a significant catalytic role in improving the dehydrogenation dynamic properties of these hydrides.

Acta Phys. -Chim. Sin. **2011,** *27* (12), 2793−2798

Effects of Cu^{2+} on Proton Transfer Processes in an Adenine-Thymine Anion Base Pair

ZHANG Feng WANG Hong-Yan
LIN Yue-Xia

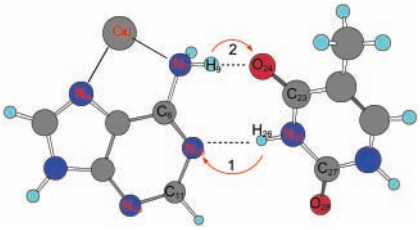

Cu^{2+} cation coordination effects on proton transfer processes in the adenine-thymine anion base pair were studied.

Acta Phys. -Chim. Sin. **2011,** *27* (12), 2799−2804

Electronic Sturctures and Optical Properties of $CuAlX_2$ (X=S, Se, Te) Semiconductors with a Chalcopyrite Structure

ZHOU He-Gen CHEN Hong
CHEN Dong LI Yi
DING Kai-Ning HUANG Xin
ZHANG Yong-Fan

Acta Phys. -Chim. Sin. **2011,** *27* (12), 2805−2813

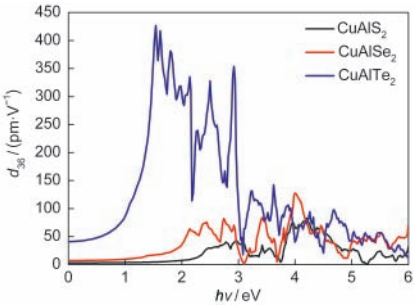

The static second harmonic generation coefficients (d_{36}) of $CuAlX_2$ (X=S, Se, Te) semiconductors increase from X=S to X=Te and values of 3.23, 7.13, and 41.19 pm·V^{-1} were obtained, respectively.

ELECTROCHEMISTRY AND NEW ENERGY

Photoinduced Electron Transfer between CdS Quantum Dots and Gold Electrodes

YUE Zhao ZHANG Wei
WANG Cheng LIU Guo-Hua
NIU Wen-Cheng

Acta Phys. -Chim. Sin. **2011,** *27* (12), 2814−2820

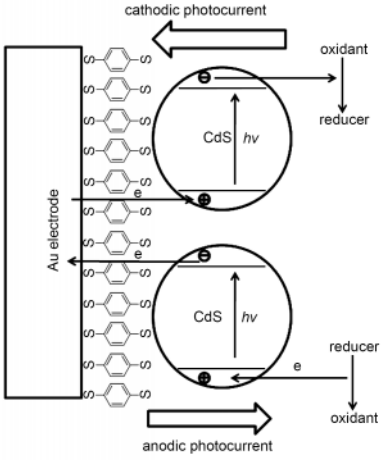

A study on the photocurrent from photoinduced electron tunneling transfer between CdS-QDs and gold electrodes for photoelectrochemical detection was carried out.

Preparation of Large Grain and Dense CdS Thin Films Using Ultrasonic Agitation Chemical Bath Deposition

SHI Cheng-Wu CHEN Zhu
SHI Gao-Yang SUN Ren-Jie

Acta Phys. -Chim. Sin. **2011,** *27* (12), 2821−2825

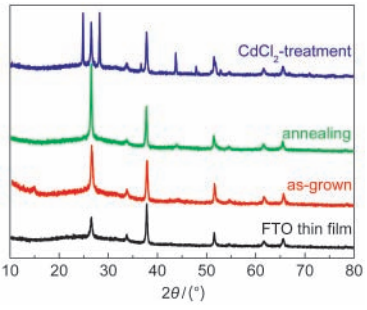

The small grains in the CdS aggregates were melted together and the CdS aggregate size did not change in UCBD-CdS thin films after the $CdCl_2$-treatment .

Preparation of CIGS Thin Films by Electrodeposition Method Using Ethanol as a Solvent

WANG Xin-Chun HU Bin-Bin
WANG Guang-Jun YANG Guang-Hong
WAN Shao-Ming DU Zu-Liang

Acta Phys. -Chim. Sin. **2011,** *27* (12), 2826−2830

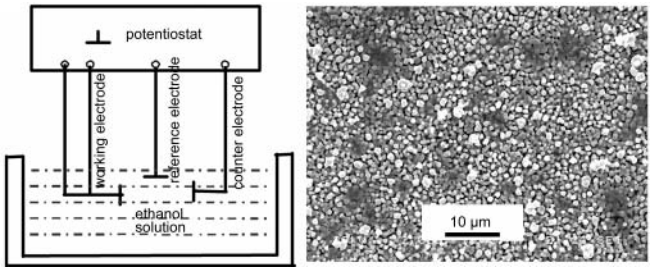

Copper indium gallium diselenide (CIGS) thin films were electrodeposited in an ethanol solution.

Photoelectrochemical Properties of Graphene Oxide Thin Film Electrodes

ZHANG Xiao-Yan SUN Ming-Xuan
SUN Yu-Jun LI Jing
SONG Peng SUN Tong
CUI Xiao-Li

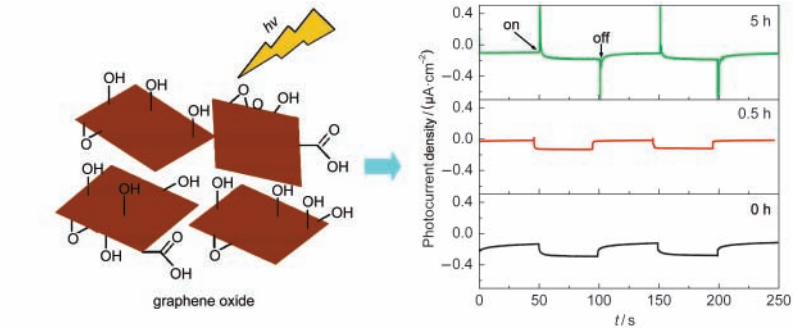

Acta Phys. -Chim. Sin. **2011,** *27* (12), 2831–2835

A series of graphene oxide thin film electrodes were prepared and their photoelectrochemical response was influenced by film thickness and UV irradiation.

Preparation and Characterization of Peanut Shell-Based Microporous Carbons as Electrode Materials for Supercapacitors

GUO Pei-Zhi JI Qian-Qian
ZHANG Li-Li ZHAO Shan-Yu
ZHAO Xiu-Song

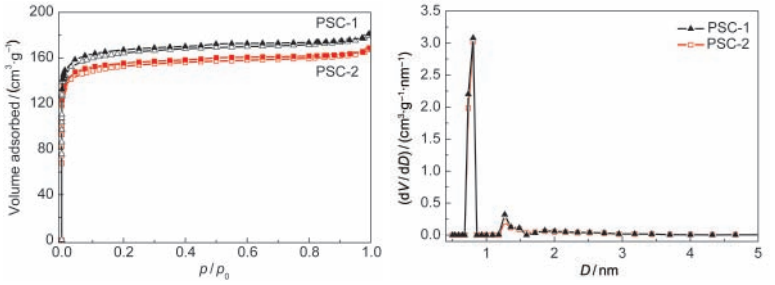

Acta Phys. -Chim. Sin. **2011,** *27* (12), 2836–2840

Microporous carbons were fabricated from the carbonization of peanut shell and they can be used as electrode materials for supercapacitors.

Inhibition Effect of Nitrotetrazolium Blue Chloride on the Corrosion of Steel in Hydrochloric Acid Solution

LI Xiang-Hong DENG Shu-Duan
FU Hui

Acta Phys. -Chim. Sin. **2011,** *27* (12), 2841–2848

Nitrotetrazolium blue chloride is a tetrazole compound that contains two tetrazole rings and acts as a good inhibitor for steel in 1.0 mol·L^{-1} HCl. It shows better inhibition performance than the tetrazole compound that contains one tetrazole ring.

Preparation of the $Ni/NiCo_2O_4$ Composite Electrode and Its Properties toward the Oxygen Evolution Reaction in Alkaline Media

BAO Jin-Zhen WANG Sen-Lin

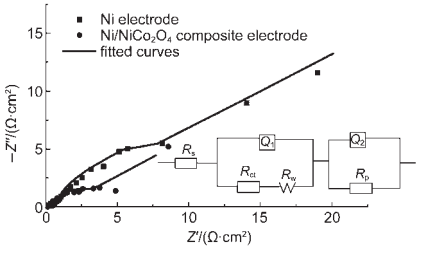

Acta Phys. -Chim. Sin. **2011,** *27* (12), 2849–2856

A $Ni/NiCo_2O_4$ composite electrode was successfully prepared by composite electrodeposition. Its electrocatalytic properties toward the oxygen evolution reaction are better than that of a nickel electrode.

PtSnCo/C Anode Catalyst for Methanol Oxidation

LI Qing-Wu WEI Zi-Dong
CHEN Si-Guo QI Xue-Qiang
LIU Xiao DING Wei
MA Yu

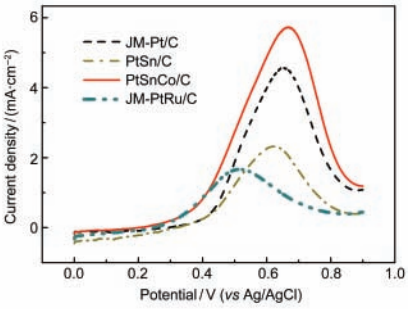

The more negative onset potential of methanol oxidation for the PtSnCo/C catalyst relative to the pre-adsorbed CO oxidation implies that the intermediates of methanol oxidation on the PtSnCo/C catalyst may be ones, which can be more easily oxidized than CO, instead of CO.

Acta Phys. -Chim. Sin. **2011,** *27* (12), 2857−2862

Preparation of Tungsten Carbide and Titania Nanocomposite and Its Electrocatalytic Activity for Methanol

HU Xian-Chao CHEN Dan
SHI Bin-Bin LI Guo-Hua

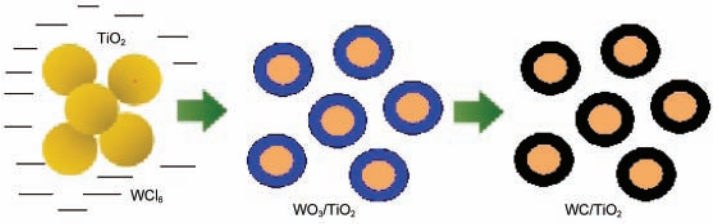

Tungsten carbide and titania nanocomposite with a core-shell structure shows good synergistic effects for the electrocatalytic oxidation of methanol.

Acta Phys. -Chim. Sin. **2011,** *27* (12), 2863−2871

CATALYSIS AND SURFACE SCIENCE

Highly Active Au/α-MnO_2 Catalysts for the Low-Temperature Oxidation of Carbon Monoxide and Benzene

YE Qing HUO Fei-Fei
YAN Li-Na WANG Juan
CHENG Shui-Yuan KANG Tian-Fang

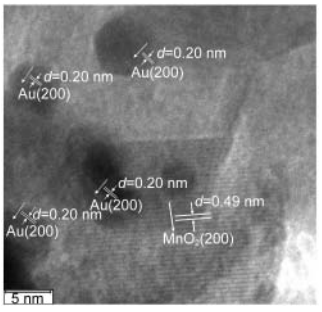

The excellent catalytic oxidation performance of xAu/α-MnO_2 was associated with highly dispersed Au, good reducibility, and synergism at the interface between the Au and MnO_2 nanodomains.

Acta Phys. -Chim. Sin. **2011,** *27* (12), 2872−2880

Hydroxylation of Benzene over V-HMS Catalysts with the Addition of Fe as the Second Metal Component

FENG Su-Jiao YUE Bin
WANG Yu YE Lin
HE He-Yong

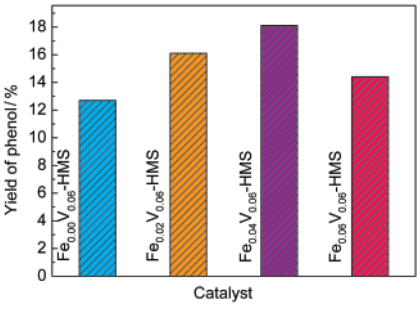

The addition of Fe as the second component can improve the catalytic activity in the hydroxylation of benzene over the V-HMS catalyst.

Acta Phys. -Chim. Sin. **2011,** *27* (12), 2881−2886

Asymmetric Hydrogenation of Acetophenone and Its Derivatives Catalyzed by L-Proline Stabilized Iridium

YANG Chao-Fen YANG Jun
ZHU Yan-Qin SUN Xiao-Dong
LI Xian-Jun CHEN Hua

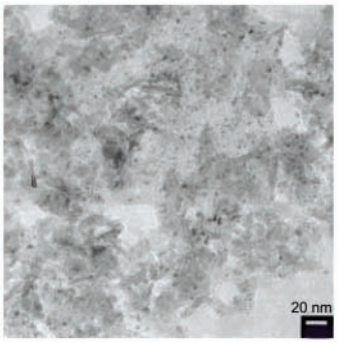

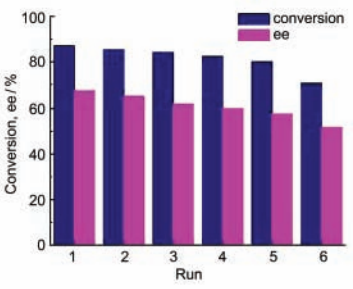

A supported iridium catalyst stabilized by L-proline exhibited good catalytic performance in the asymmetric hydrogenation of acetophenone and its derivatives.

Acta Phys. -Chim. Sin. **2011,** *27* (12), 2887–2892

Synthesis, Characterization of SSZ-33 Molecular Sieves and Their Performance for the Automobile Tailpipe Hydrocarbon Trap

PAN Rui-Li FAN Wei-Bin
LI Yu-Ping LI Xiao-Feng
LI Sha DOU Tao

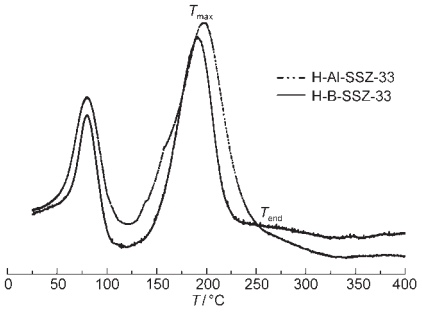

The synthesis of Al-SSZ-33 was achieved by a post-modification procedure of B-SSZ-33 molecular sieves in an $Al(NO_3)_3$ solution. The synthesized material is a novel catalyst for use as a hydrocarbon trap in automobile tailpipes.

Acta Phys. -Chim. Sin. **2011,** *27* (12), 2893–2899

PHOTOCHEMISTRY AND RADIATION CHEMISTRY

Effect of Oxygen Vacancy on the Optical Properties of Porous Zirconia

OUYANG Jing SONG Xing-Lin
LIN Ming-Yue ZOU Ju
LI Jing-Jing ZHU Jiang-Ping
YANG Hua-Ming

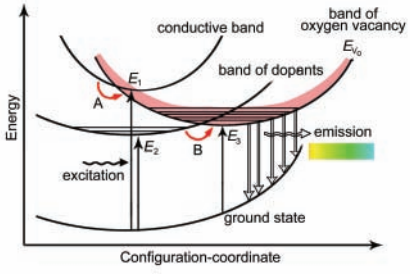

Oxygen vacancies in porous ZrO_2 lead to a combination of excitation and dopant states and dominate the luminescent emissions.

Acta Phys. -Chim. Sin. **2011,** *27* (12), 2900–2906

BIOPHYSICAL CHEMISTRY

Interactions between Different Classes of Surfactants and Metmyoglobin

ZHANG Ying-Ying CAO Hong-Yu
TANG Qian ZHENG Xue-Fang

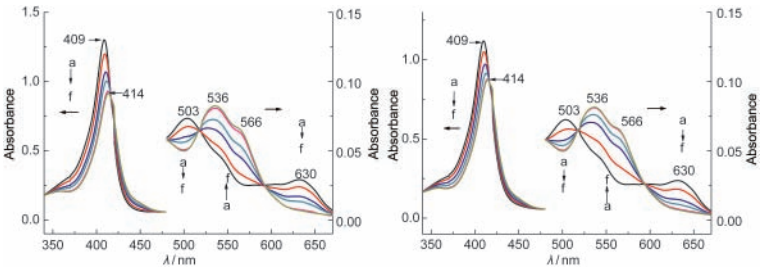

The effects of different classes of surfactants on the UV-Vis absorbance spectra of metMb were investigated.

Acta Phys. -Chim. Sin. **2011,** *27* (12), 2907−2914

PHYSICAL CHEMISTRY OF MATERIALS

Structure and Morphology of Induction-Melted Higher Manganese Silicide

ZHOU Ai-Jun CUI Heng-Guan
LI Jing-Ze ZHAO Xin-Bing

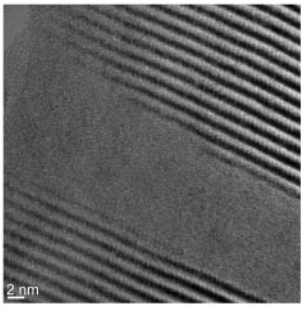

Amorphous MnSi striations were observed in induction-melted higher manganese silicide (HMS), which was determined as single phase Mn_4Si_7 by SAED. Hot-pressing of HMS powders led to a substantial change in microstructure.

Acta Phys. -Chim. Sin. **2011,** *27* (12), 2915−2919

Synthesis and Characterization of Sphere-Like Cu_2ZnSnS_4 Nanocrystals by Solvothermal Method

CAI Qian LIANG Xiao-Juan
ZHONG Jia-Song SHAO Ming-Guo
WANG Yun ZHAO Xiao-Wei
XIANG Wei-Dong

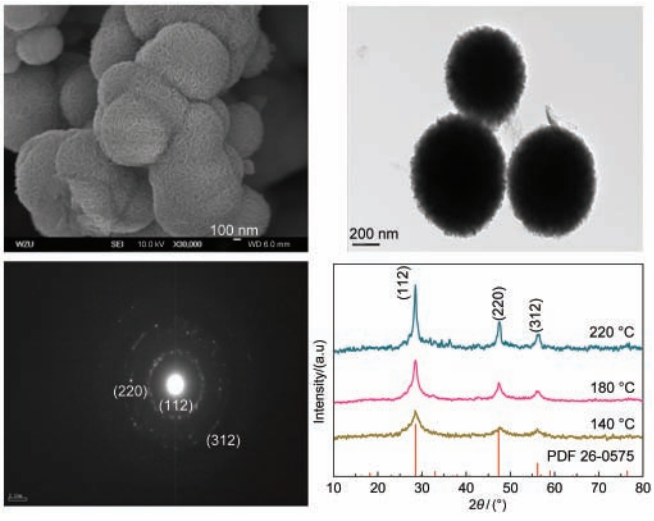

Sphere-like Cu_2ZnSnS_4 nanocrystals were synthesized by a L-cysteine-assisted solvothermal route. The phase, structure, morphology, and optical properties were also characterized.

Acta Phys. -Chim. Sin. **2011,** *27* (12), 2920−2926

Formation Mechanism of Barium Titanate Nanoparticle Aggregations

ZHAN Hong-Quan JIANG Xiang-Ping
LI Xiao-Hong LUO Zhi-Yun
CHEN Chao LI Yue-Ming

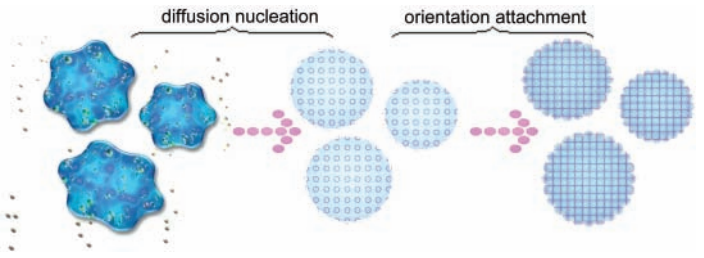

$BaTiO_3$ nanoparticle aggregates have been grown from barium hydroxide and titanium butoxide by the hydrothermal method. The aggregates have been crystallized in the cubic phase. The growth of the barium titanate nanoparticles aggregation follows the “diffusion nucleation – orientation attachment” formation mechanism.

Acta Phys. -Chim. Sin. **2011,** *27* (12), 2927−2932

Microwave-Assisted Hydrothermal Synthesis of Ag-Loaded Titania Nanotubes and Their Photocatalytic Performance

CHEN Shu-Hai XU Yao
LÜ Bao-Liang WU Dong

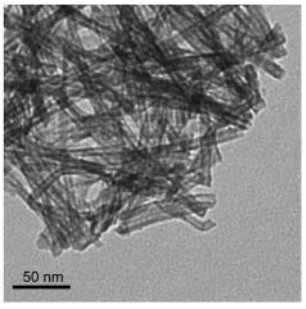

Titania nanotubes were synthesized by the microwave-assisted hydrothermal method and loaded with Ag to enhance their visible light photocatalytic activity.

Acta Phys. -Chim. Sin. **2011,** *27* (12), 2933−2938

Facile Synthesis of Assembly HAP Nanoribbon Spheres and the Synergized Action of Its Photocatalytic Properties

YANG Xiao-Hong LIU Chang
LIU Jin-Ku ZHU Zi-Chun

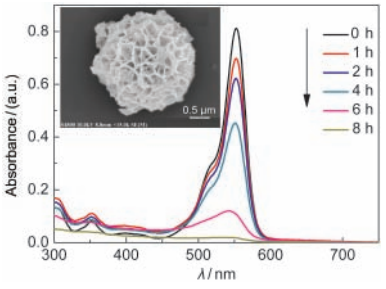

HAP nanoribbon assembly spheres with a high surface area were prepared by a facile and efficient cooperation template method. The degradation rate of rhodamine B increased by 125% when using the composite as a catalyst compared with using ZnO nanoparticles.

Acta Phys. -Chim. Sin. **2011,** *27* (12), 2939−2945

Adjustable Synthesis and Visible-Light Responsive Photocatalytic Performance of $V_2O_5 \cdot xH_2O$-$BiVO_4$ Nanocomposites

LI Ben-Xia WANG Yan-Fen
LIU Tong-Xuan

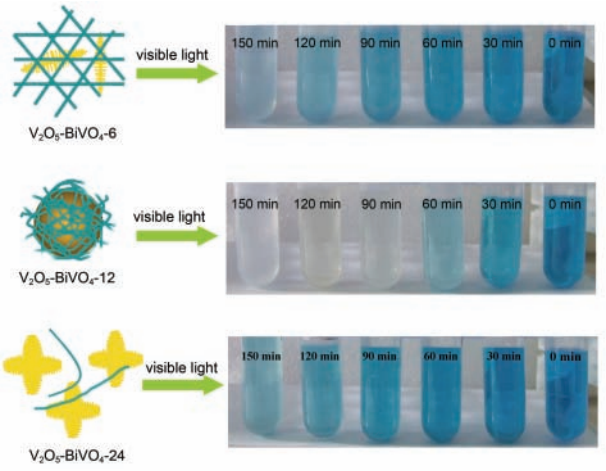

Acta Phys. -Chim. Sin. **2011,** *27* (12), 2946–2952

The synthesis-time-dependent microstructures and photocatalytic performance of $V_2O_5 \cdot xH_2O$-$BiVO_4$ composites were investigated.

Direct Graphene Growth by Depositing Carbon Atoms on Si Substrate Covered by SiC Buffer Layers

TANG Jun KANG Chao-Yang
LI Li-Min XU Peng-Shou

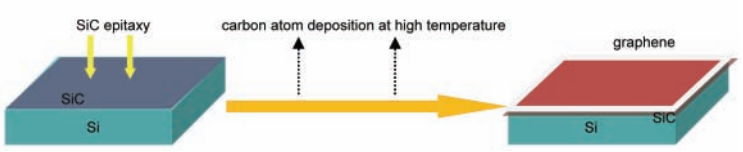

Acta Phys. -Chim. Sin. **2011,** *27* (12), 2953–2959

Graphene thin films were grown on Si substrates covered by SiC buffer layers with the method of directly depositing carbon atoms.

NEWS AND COMMENTS